Version of Record: https://www.sciencedirect.com/science/article/pii/S0168583X22000155
Manuscript_95e6e241150971d78a8b046c4005e2dd

Thick target neutron yields from Beryllium, Carbon, Tungsten, and Lead targets irradiated by 26.7 MeV/nucleon ^4He ions

X. Zhang[a,b,c], Z. Chen[a,b,c,*], R. Wada[d], R. Han[a,b,c], G. Tian[a,c], B. Liu[a,b,c], F. Shi[a,c], H. Sun[a,b,c]

[a]*Institute of Modern Physics, Chinese Academy of Sciences, Lanzhou, 730000, China*
[b]*School of Nuclear Science and Technology, University of Chinese Academy of Science, Beijing 100049, China*
[c]*Advanced Energy Science and Technology Guangdong Laboratory, Huizhou, 516000, China*
[d]*Cyclotron Institute, Texas A&M University,College Station, Texas 77843, USA*

Abstract

The angular and energy distributions of secondary neutrons produced from 26.7 MeV/nucleon ^4He ions, stopping in thick Be, C, W and Pb targets are measured by the time of flight method. The GEANT4, PHITS, and FLUKA Monte Carlo simulation codes with different physics models are employed to simulate the neutron yields and the results are compared with the experimental data. For the thick Be and C targets, GEANT4 with INCL++ reproduces the experimental data reasonably well. Whereas PHITS with JQMD-2.0 overestimates the neutron yields at intermediate energies and FLUKA with PEANUT underestimated the neutron yields at intermediate energies. For W and Pb targets, FLUKA with PEANUT physics model agree with experimental data best. PHITS with JQMD-2.0 overestimates the neutron yield at intermediate energies at 0°, and GEANT4 with INCL++ underestimates the neutron yield at intermediate energies at three angles.

Keywords: Thick target neutron yields, ^4He ions, GEANT4, PHITS, FLUKA

1. Introduction

The energy and angular distributions of thick target neutron yield (TTNY) from α-induced reactions are important for different applications, including ion therapy, shielding of accelerator facilities, and space radiation protection[1]. In ion therapy, ^4He ions are often used to reduce the radiation damage to healthy tissues, because of its smaller projectile fragmentation yields and smaller spreading of the beam along their path[2], compared to gamma ray or proton beams. To design the radiation shielding of ion accelerators, neutron yield should be known accurately due to its high penetrability and biological damage. For deep-space missions, the helium component of the primary particles in the Solar Energetic

*Corresponding author
Email address: zqchen@impcas.ac.cn (Z. Chen)

© 2022 published by Elsevier. This manuscript is made available under the Elsevier user license
https://www.elsevier.com/open-access/userlicense/1.0/

Particles (SEP) and Galactic Cosmic Rays (GCR) makes significant contributions to the total astronaut radiation exposure[3]. The neutrons from interactions of the primary ^4He ions with shielding materials also generate a radiation field which causes risks for long-term space missions. Therefore, data on the secondary neutrons from a thick target are crucial to protect person and equipments.

The Monte Carlo simulation codes, such as GEANT4[4, 5], PHITS[6, 7], FLUKA[8], and MCNP[9], have been recently used for simulating thick target neutron yields. These transport codes predict neutron yields rely on accurate cross section data and nuclear reaction models. The emitted neutrons data from thick targets not only can be used to validate simulated results, but also improve the physics models implemented in these simulation codes. However, the thick target neutron yields data from ^4He ions are very scarce in the energy range of about 20 MeV/nucleon[10–14], and the data are still limited for the targets related to the space applications.

To provide needed data for the variety of applications, we measured the angular and energy distributions of neutron produced from thick Be, C, W, and Pb targets bombarded by ^4He projectile with 26.7 MeV/nucleon. The results are compared with those obtained from the GEANT4, PHITS, and FLUKA Monte Carlo simulation codes.

2. Experimental method

2.1. Experimental setup

The experiment was performed on the Radioactive Ion Beam Line (RIBLL)[15] in Lanzhou at the Institute of Modern Physics, China. The experimental arrangement is schematically shown in Fig.1. The beam spot was monitored by a remote-controlled fluorescent target for the monitor of the beam position. Counts of incident beam particles were continuously monitored by a 0.5-mm thick plastic scintillator detector which was placed at 67cm upstream from the target in a vacuum chamber and labeled TP in Fig.1.

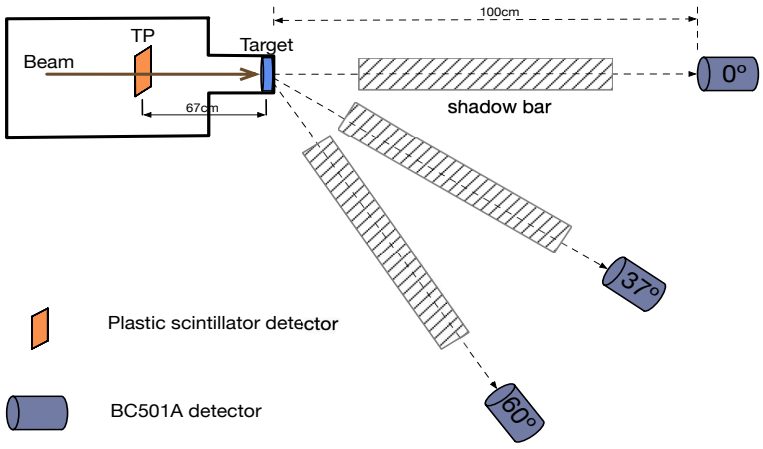

Figure 1: Schematic presentation of the experimental setup

Table 1: Details of the stopping targets

Target	Radius (mm)	thickness (mm)	Range for ^4He (mm)	R/t ratio
beryllium	35	5.08	3.897	0.767
carbon	50	5.0	2.967	0.593
tungsten	50	2.0	0.903	0.452
lead	50	3.0	1.607	0.536

The primary ^4He ions were fully stopped in the cylindrical target. The ranges of ^4He ions in thick Be, C, W, and Pb targets were calculated with SRIM-2013 code[16]. The SRIM results for ^4He ions and the target dimensions are listed in Table 1. The target was attached on the exit flange which was made by 3-mm thick of pure iron plate.

The secondary particles produced by ^4He-induced reactions with these targets include neutrons, photons and light charged particles. After exiting the 3-mm thick iron window, only neutrons and few high-energy protons can go through the window. These protons are considered in the data process. Three BC501A organic liquid scintillation detectors were employed to measure the secondary neutrons at 0°, 37°, and 60° with respect to the beam direction in the laboratory frame. All the BC501A detectors have identical cylindrical shape with areal size of 12.7-cm diameter and 12.7-cm long.

The background neutrons came from secondary neutrons scattered by the wall and other structural materials in the measurement room. To evaluate the background neutrons contribution, shadowbar correction was performed. Measurements were conducted with and without the iron shadowbars which was inserted in the flight path from the target to the detectors. The shadowbars were 15 cm by 15 cm square and 90-cm long which were placed in the front of detectors and fully block the direct neutrons from the target and allowed only background neutrons to enter the detector. The background neutrons were measured using the three shadowbars for all detectors in one run.

2.2. Electronics and data acquisition

A schematic diagram of the electronics for the experiment is shown in Fig.2. The signals from the plastic scintillator detector were split into two, one was delayed and given into a QDC module to obtain the pulse height spectrum of primary ^4He ions to filter pileup events. The other was put into a CFD module. One of the CFD outputs was given into the Scaler module to count the number of incident beam particles. Another output signal was fed into a coincidence module with OR of the BC501A signals to generate the master trigger signal. The signal was also fed into a scaler module to obtain the number of the triggered events. The rest of output signals was delayed and fed into a TDC module to serve as the stop signal in the time of flight measurements (TOF). The anode signal from BC501A liquid scintillation detector was also split into three. One was put into a CFD module, and one of the CFD output was fed into the TDC module as start signals for the TOF measurements, and the other was fed into a coincidence module. Two of the split signals were delayed with

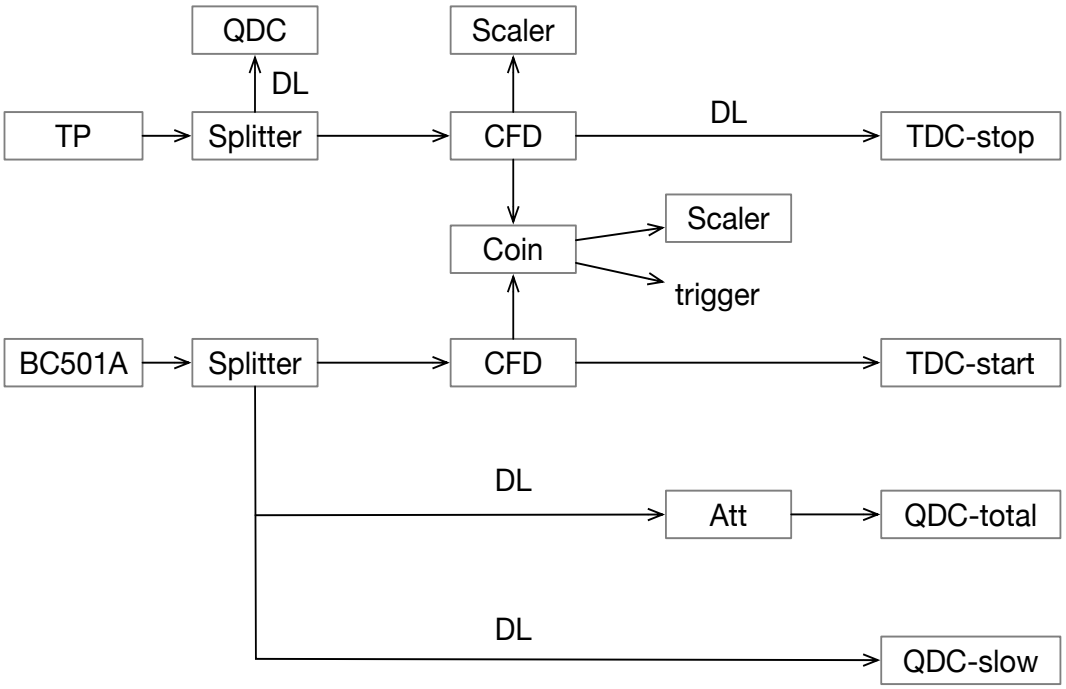

Figure 2: simplified logic diagram for the electronics

different delay times and fed into a QDC module for pulse shape discrimination.

3. Data analysis

ROOT-v6.22/03[17] developed in the European Organization for Nuclear Research (CERN) was used in the offline data analysis. The energy distributions of the secondary neutrons were deduced from the TOF measurement, and the neutrons were separated from photons by using the pulse shape discrimination method.

3.1. Energy calibration and neutron-detection efficiency

Accurate data of the pulse height response to recoil proton energy is needed in the neutron efficiency of the neutron detectors. Gamma-ray sources, ^{22}Na, ^{60}Co, and ^{137}Cs, were used for experimentally obtaining the relationship between the certain location in the pulse height spectrum and the Compton electron energy, and then converting the electron equivalent energy to the recoil proton energy. To get the precise electron equivalent energy corresponding to the peak in the Compton spectra, GEANT4 was employed to examine the light-output spectra in the experimental condition. Neutron-detection efficiencies of the BC501A liquid organic scintillators are very important to determine neutron spectra. Detection efficiencies are calculated by SCINFUL-QMD code[18], which is integrated in PHITS. SCINFUL-QMD code has been benchmarked and used in neutron detector efficiency calculations in previous works[10, 14, 19–22]. This code can calculate the light-output in the nuclear reaction between neutrons and scintillator materials by using SCINFUL[23] physics

model below 80 MeV and QMD physics model above 80 MeV. The light-output spectra were integrated above a threshold level to get the detection efficiency. The threshold level was set at the position of half height with respect to a Compton edge in a measured light-output distribution with photons from the radioisotope sources of ^{60}Co, and ^{137}Cs. Fig.3 shows the neutron-detection efficiencies by SCINFUL-QMD with the threshold levels of ^{60}Co, and ^{137}Cs.

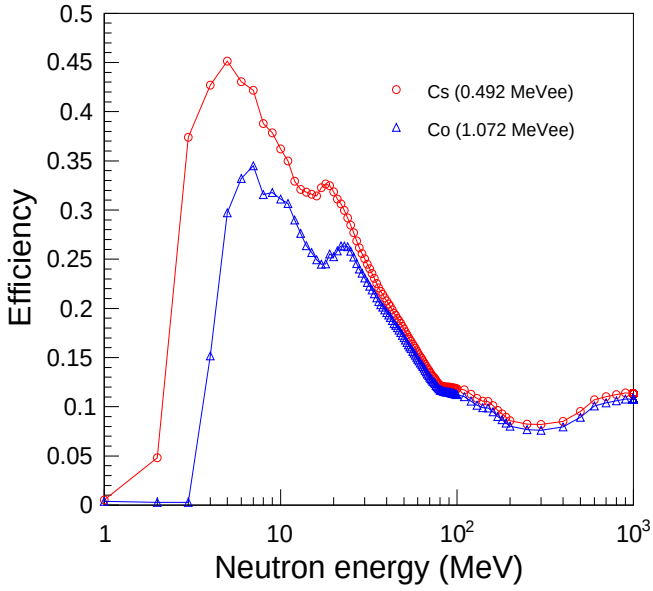

Figure 3: The efficiency of BC501A detector obtained by SCINFUL-QMD code with the threshold levels of 0.492, 1,072 MeVee

3.2. Discrimination of events

Neutrons were distinguished from photons by using the pulse shape discrimination method (PSD). The PSD uses two QDC data from total and slow time gates and a typical result is shown in Fig.4. Charged particles, mainly protons, are at the lower band and non-charged particles, neutrons and gammas, are at the upper band. There is an overlap region between the gammas and neutrons in the upper band for the lower pulse height, as shown in the figure. The lines depicted in Fig.4 indicate the threshold level of ^{60}Co (1.072 MeVee), and ^{137}Cs (0.492 MeVee), which corresponds to 1.8 MeV and 3.0 MeV in neutron energy. The energy threshold of each detector was set at the threshold level of ^{60}Co which successfully distinguish the neutron events from the photon events.

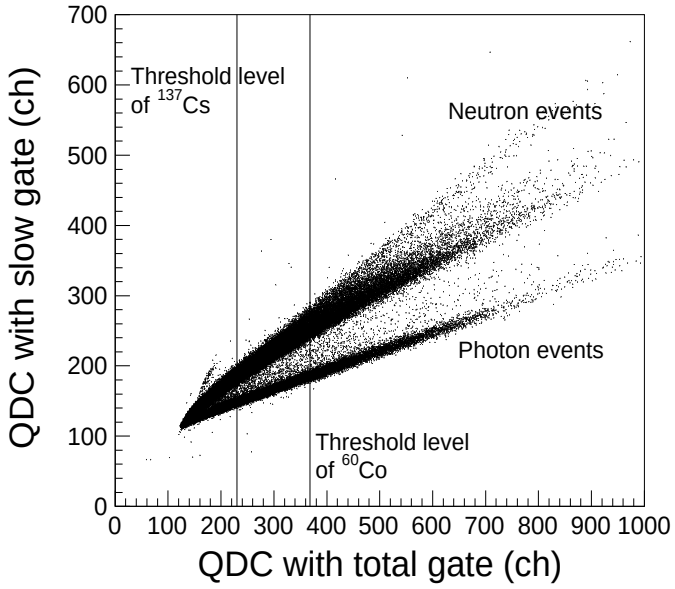

Figure 4: Result of PSD by the two-gate integration method

3.3. Double differential thick target neutron yields

The neutron energy was calculated from the TOF spectrum using the following formula:

$$E = \left(\frac{1}{\sqrt{1-\left(\frac{L}{t_{n-\gamma}c+L}\right)^2}} - 1\right)m_n c^2 \tag{1}$$

where E is the kinectic energy of neutron, γ is the Lorentz factor, L is the flight path, $t_{n-\gamma}$ is the flight time difference between the prompt γ-ray and the neutron, $m_n c^2$ is the rest mass of the neutron, c is the velocity of light in vacuum. The energy resolution and the uncertainty in the time of flight measurements was reported in [20], and is given by

$$\frac{\Delta E}{E} = \gamma(\gamma+1)\frac{\Delta t}{t_{n-\gamma}} \tag{2}$$

Here, $\Delta E/E$ is the energy resolution, Δt is the time resolution. The time resolution consists of the intrinsic detector time resolution, the intrinsic time resolution of the beam and the flight path variation due to interaction point position within the finite size of the detector. The time resolution of 1.5ns is was estimated from the Full Width at Half Maximum (FWHM) of the prompt gamma-ray peak. The energy resolution is evaluated and shown in Fig.5.

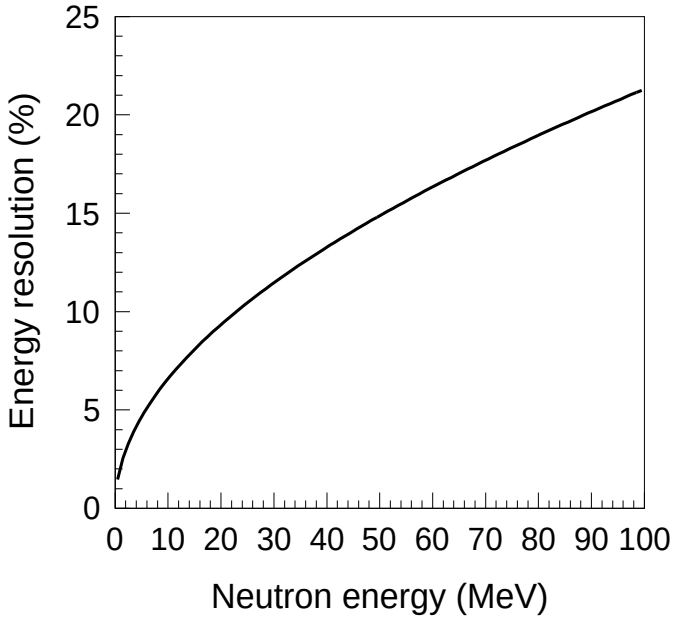

Figure 5: The energy resolution as a function of neutron energy for the experiment.

The double-differential thick-target neutron yields is derived from the following equation,

$$\frac{d^2Y}{dEd\Omega} = \frac{N_n}{N_{ion} \cdot \epsilon \cdot \Delta E \cdot \Delta\Omega} \tag{3}$$

where N_n is the number of detected neutrons, N_{ion} is the number of incident ^4He ions, ϵ is the neutron detection efficiency, ΔE is the energy bin width, and $\Delta\Omega$ is the solid angle subtended by the neutron detector. The results of the TTNY are obtained by subtracting the background data measured with the shadow bars. The uncertainty of the experimental data mainly originates from the statistical errors and the uncertainties of the effective solid angle and the calculated detector efficiencies. The statistical errors were less than 5% at energies below 20 MeV and increased to 35% at high-energy end from the neutron counts. The uncertainty in solid angle acceptance was less than 13% in all cases. The uncertainty of the detection efficiency is estimated to be less than 10% for the incident neutron-energy range of 0.1-80 MeV[23], and slightly exceeds 10% with higher energy neutrons[21]. We set the overall uncertainty of the neutron detection to 15% in the analysis. The attenuation of neutron fluence after passing through the air and the exit window were calculated by the GEANT4 simulation tool. The magnitudes of attenuation for exit window was less than 5% for the energy range of 1-20 MeV, and less than 1% for above 20 MeV. The air attenuation was less than 1%. The attenuation corrections have been applied to the experimental data.

4. The Monte Carlo codes

4.1. GEANT4

GEANT4 is an open-source Monte Carlo simulation toolkit used to simulate particles transportation and interaction through matter. It is widely used in a wide range of application domains, including high energy physics, space science, medical physics and radiation protection. The GEANT4.10.6-p02 has been used in this work. GEANT4 provides interfaces to enable various physics models. The physics list QGSP_INCLXX_HP is used for the calculations. In the Liege intranuclear cascade model INCL++[24], nucleons are initialized as a free Fermi gas in a static potential well. In the collision process, nucleons from the projectile overlapped with the target volume are labeled as participants, and the rest of the projectiles are assigned as a quasi-projectiles. The quasi-target is same as the quasi-projectiles in the center of mass system, but fly away in the opposite direction. The final state of the quasi-target is determined by the full collision dynamics of the cascade. The de-excitation of the excited nucleus is treated by the G4Excitationhandler statistical de-excitation model. This class manages five different de-excitation models, including the evaporation implemented according to the Weisskopf-Ewing model, and the Fermi break-up model. The simulations are taken into account the geometry of the experimental set up described in Section 2, and made with three virtual detectors at $\theta = 0°$, $37°$, $60°$ for each target. These conditions are same for other two simulations described below.

4.2. PHITS

PHITS is a Monte Carlo particle transport simulation code developed under the collaboration between JAEA, RIST, KEK and several other institutes. The PHITS code version 3.24 is utilized for the calculations in this work. Using precise physics models and the evaluated nuclear data libraries, it can simulate particle transport in wide energy ranges and has been applied in different research fields, including radiation shielding, medical physics, and radiological protection. For ^{4}He-induced reactions, JAERI Quantum Molecular Dynamics 2.0 (JQMD-2.0)[25] physics model was used for A-A collisions in this work. JQMD-2.0 describes A-A reactions more reasonable than the JQMD model, particularly for peripheral collisions. In the JQMD-2.0 model, each nucleon is described by a Gaussian wave function which is propagated inside the nuclear medium. Different from INCL++ model, all nucleons are treated equally without the spectator-participant concept. The particles are propagated and interact through an effective nucleon-nucleon interaction. The evaporation and fission are treated using the Generalized Evaporation Model (GEM) is adopted for simulating the statistical decay process at the later stage for nucleus-induced reactions. A T-track section was used to record secondary neutrons which hit the virtual detectors.

4.3. FLUKA

FLUKA is a Monte Carlo tool for the calculations of particle transport and interactions with matter. The FLUKA code version 4-1.1 is used for the calculations. It treats A-A interactions with the Boltzmann Master Equation (BME) at energy below 125 MeV/nucleon, and for energies between 125 MeV/nucleon to 5 GeV/nucleon, the modified Relativistic

Quantum Molecular Dynamics model (RQMD) is used. Since the RQMD and BME models only deal with the early stage of a nucleus-induced reaction, excited fragments produced from the RQMD and BME models are further processed by the PEANUT which includes the Generalized IntraNuclear Cascade (GINC) and a preequilibrium stage, followed by evaporation/fission or Fermi break-up, and gamma de-excitation. For light equilibrium compound nuclei ($A \leq 16$), the evaporation-fission stage is replaced by Fermi break-up. At the end of the reaction stage, gamma de-excitation is performed when particle emission is no longer energetically possible. In the calculation PRECISIOn mode is used. A USRYIELD tally card is also utilized in the calculation.

5. Results and discussion

The experimental double-differential thick-target neutron yields (TTNY) from the 26.7 MeV/nucleon ^4He bombarding on the Be, C, W, and Pb targets are shown in Fig.6 through Fig.9 with the simulation results. The experimental data are presented with square dots, and the GEANT4, PHITS and FLUKA simulation results are in solid dots with green, red, and blue color respectively. To compare the spectra at all measured angles in a plot, the energy spectra are scaled by different factors, indicated for each angle in the plot. The spectrum at 0° is scaled by a factor of 1 and is reduced by a factor of 10^{-3} with the increasing each angle. The error bars represented the statistical uncertainties associated with the measurements.

In the spectrum, neutrons at a peak around 26 MeV in the forward angle are mainly from the directly peripheral collisions between the neutrons in a projectile and nucleons from a target nucleus. The peak energy approaches the projectile energy per nucleon, and is broadened for heavy nuclei target. At the tail of this peak on the higher energy side, neutrons energy becomes up to several times of the incoming beam energy per nucleon could be produced by Fermi motion effect in collisions. At intermediate energies at the larger angles, neutrons are mainly from the pre-equilibrium emission of the composite system created by the overlap of the projectile and target nuclei. Below around 15 MeV, the spectra contain the isotropically emitted neutrons which originate from the de-excitation of excited target residues and fragments in the equilibrium process.

From the comparisons, it is observed that disagreements exist not only between the experimental data and the simulations but also between the different model calculations. Only the spectra from GEANT4 with INCL++ physics model reveals the peak structure at 0° and reproduce well the experimental data for Be and C targets. However, it slightly underestimates the low energy neutron yields contributed from the evaporation of excited target residues and fragments, and also significantly underestimates the intermediate energy neutrons for W and Pb targets. The results from FLUKA with PEANUT physics model reproduces the experimental data best for W and Pb targets except at 60 degree for W target. However, it overestimates the neutron yield at energy region below 10 MeV for Be target at 0° and C target, and underestimates at high energies for Be and C targets significantly above 30 MeV for Be and 50 MeV for C target. For the spectra from PHITS with JQMD-2.0 physics model, it overestimates the neutron production significantly at intermediate energies at 0° for all targets. And the discrepancies reduces at 37° for Be and C targets. But for

W and Pb targets, it reproduced the experimental data reasonably well at larger angles. At high energy tail, it show underestimates for Be and C targets, which is similar to those observed for the FLUKA results.

Fig.10 shows the calculations over Experimental data ratios (C/E) of the angular yields at each measured angle integrated over the entire hemisphere with the three Monte Carlo simulation codes. The C/E values for all targets at three angles are less than a factor of 3 except the PHITS calculation for C target at 0°. The trend of the C/E ratios of the angular yields corresponds to the TTNY spectra. Particularly, PHITS with JQMD-2.0 model show higher value at 0° for all targets, while GEANT4 with INCLXX model show lower value.

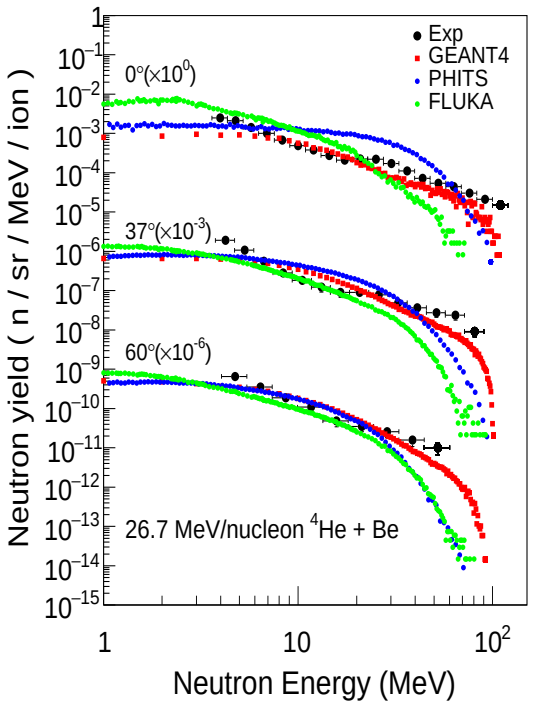

Figure 6: Double differential neutron yield for thick Be target

6. Conclusion

The measurement of secondary neutrons created by 26.7 MeV/nucleon ^4He ions bombarding on thick Be, C, W, and Pb targets are performed. The emitted neutrons were measured at 0°, 37°, 60°. Three Monte Carlo simulation tools, GENT4, PHITS, and FLUKA with different physics models were used to calculate the thick target neutron yields.

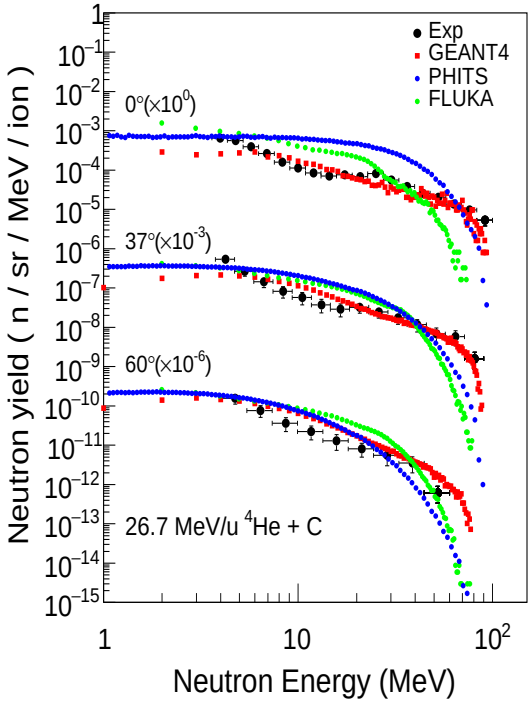

Figure 7: Double differential neutron yield for thick C target

From the comparison with experimental data, none of the calculated results agree well with the experimental data. For Be and C targets, however, GEANT4 with INCL++ model reproduced the peak structure as in experimental data. While PHITS with JQMD-2.0 overestimated the neutron yields at intermediate energies and FLUKA with PEANUT underestimated the neutron yields at intermediate energies. For W and Pb targets, FLUKA with PEANUT physics model match the experimental data best. PHITS with JQMD-2.0 overestimated the neutron yield at intermediate energies at 0°, and GEANT4 with INCL++ underestimate the neutron yield at intermediate energies at three angles. In overall when the lighter target materials dominate the evaluated sample, GEANT4 with INCL++ works well. When the heavier marterials are dominated, FLUKA with PEANUT works best. For further work, the physics models used for thick target neutron yields calculation need improvements. And more experiments need to be performed with important materials at large degree.

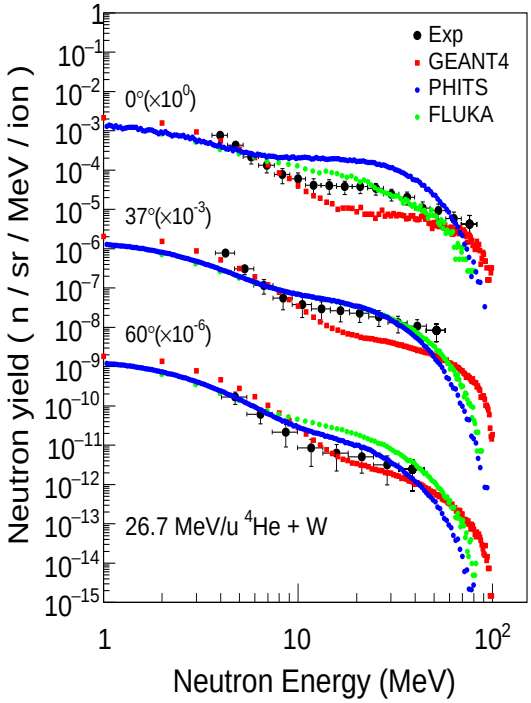

Figure 8: Double differential neutron yield for thick W target

Acknowledgments

This study was supported by the National Natural Science Foundation of China (Grant Nos. 11875298 and U1832205) and the US Department of Energy under Grant No. DE-FG02-93ER40773. We appreciate greatly the skillful work of the RIBLL operation staff. The authors are also thankful to Dr. Takuya Furuta and Dr. Daiki Satoh of Japan Atomic Energy Agency for supporting for the SCINFUL-QMD calculations.

References

[1] J. W. Norbury, G. Battistoni, J. Besuglow, L. Bocchini, D. Boscolo, A. Botvina, M. Clowdsley, W. de Wet, M. Durante, M. Giraudo, T. Haberer, L. Heilbronn, F. Horst, M. Krämer, C. La Tessa, F. Luoni, A. Mairani, S. Muraro, R. B. Norman, V. Patera, G. Santin, C. Schuy, L. Sihver, T. C. Slaba, N. Sobolevsky, A. Topi, U. Weber, C. M. Werneth, C. Zeitlin, Are further cross section measurements necessary for space radiation protection or ion therapy applications? helium projectiles, Frontiers in Physics 8 (2020) 409. doi:10.3389/fphy.2020.565954.
URL https://www.frontiersin.org/article/10.3389/fphy.2020.565954

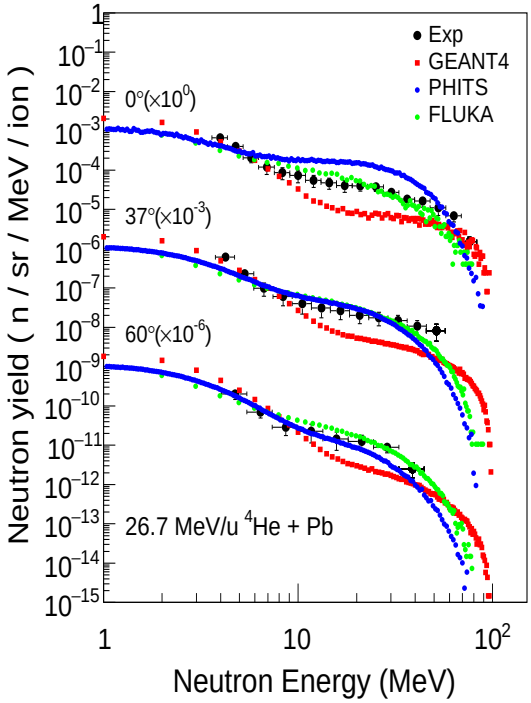

Figure 9: Double differential neutron yield for thick Pb target

[2] F. Tommasino, E. Scifoni, M. Durante, New Ions for Therapy, International Journal of Particle Therapy 2 (3) (2016) 428–438. arXiv:https://meridian.allenpress.com/theijpt/article-pdf/2/3/428/2007101/ijpt-15-00027_1.pdf, doi:10.14338/IJPT-15-00027.1.
URL https://doi.org/10.14338/IJPT-15-00027.1

[3] J. W. Norbury, T. C. Slaba, S. Aghara, F. F. Badavi, S. R. Blattnig, M. S. Clowdsley, L. H. Heilbronn, K. Lee, K. M. Maung, C. J. Mertens, J. Miller, R. B. Norman, C. A. Sandridge, R. Singleterry, N. Sobolevsky, J. L. Spangler, L. W. Townsend, C. M. Werneth, K. Whitman, J. W. Wilson, S. X. Xu, C. Zeitlin, Advances in space radiation physics and transport at nasa, Life Sciences in Space Research 22 (2019) 98–124. doi:https://doi.org/10.1016/j.lssr.2019.07.003.
URL https://www.sciencedirect.com/science/article/pii/S2214552419300495

[4] S. Agostinelli, J. Allison, K. Amako, J. Apostolakis, H. Araujo, P. Arce, M. Asai, D. Axen, S. Banerjee, G. Barrand, F. Behner, L. Bellagamba, J. Boudreau, L. Broglia, A. Brunengo, H. Burkhardt, S. Chauvie, J. Chuma, R. Chytracek, G. Cooperman, G. Cosmo, P. Degtyarenko, A. Dell'Acqua, G. Depaola, D. Dietrich, R. Enami, A. Feliciello, C. Ferguson, H. Fesefeldt, G. Folger, F. Foppiano, A. Forti, S. Garelli, S. Giani, R. Giannitrapani, D. Gibin, J. Gómez Cadenas, I. González, G. Gracia Abril, G. Greeniaus, W. Greiner, V. Grichine, A. Grossheim, S. Guatelli, P. Gumplinger, R. Hamatsu, K. Hashimoto, H. Hasui, A. Heikkinen, A. Howard, V. Ivanchenko, A. Johnson, F. Jones, J. Kallenbach, N. Kanaya, M. Kawabata, Y. Kawabata, M. Kawaguti, S. Kelner, P. Kent, A. Kimura, T. Kodama, R. Kokoulin, M. Kossov, H. Kurashige, E. Lamanna, T. Lampén, V. Lara, V. Lefebure, F. Lei, M. Liendl, W. Lock-

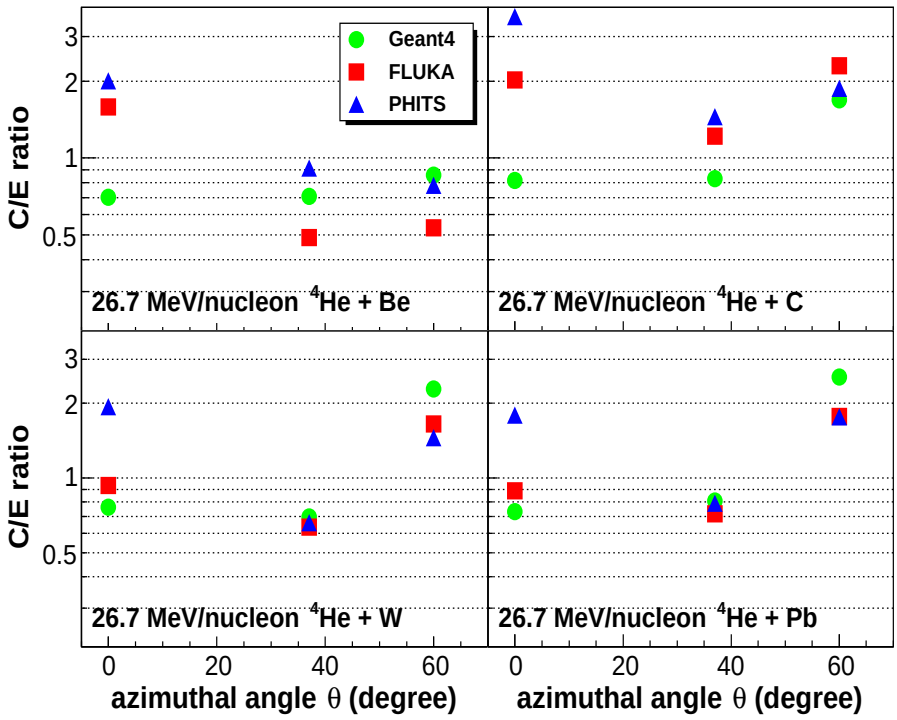

Figure 10: The calculation-to-experiment ratios of the angualr neutron yields

man, F. Longo, S. Magni, M. Maire, E. Medernach, K. Minamimoto, P. Mora de Freitas, Y. Morita, K. Murakami, M. Nagamatu, R. Nartallo, P. Nieminen, T. Nishimura, K. Ohtsubo, M. Okamura, S. O'Neale, Y. Oohata, K. Paech, J. Perl, A. Pfeiffer, M. Pia, F. Ranjard, A. Rybin, S. Sadilov, E. Di Salvo, G. Santin, T. Sasaki, N. Savvas, Y. Sawada, S. Scherer, S. Sei, V. Sirotenko, D. Smith, N. Starkov, H. Stoecker, J. Sulkimo, M. Takahata, S. Tanaka, E. Tcherniaev, E. Safai Tehrani, M. Tropeano, P. Truscott, H. Uno, L. Urban, P. Urban, M. Verderi, A. Walkden, W. Wander, H. Weber, J. Wellisch, T. Wenaus, D. Williams, D. Wright, T. Yamada, H. Yoshida, D. Zschiesche, Geant4—a simulation toolkit, Nuclear Instruments and Methods in Physics Research Section A: Accelerators, Spectrometers, Detectors and Associated Equipment 506 (3) (2003) 250–303. doi:10.1016/S0168-9002(03)01368-8. URL https://www.sciencedirect.com/science/article/pii/S0168900203013688

[5] J. Allison, K. Amako, J. Apostolakis, P. Arce, M. Asai, T. Aso, E. Bagli, A. Bagulya, S. Banerjee, G. Barrand, B. Beck, A. Bogdanov, D. Brandt, J. Brown, H. Burkhardt, P. Canal, D. Cano-Ott, S. Chauvie, K. Cho, G. Cirrone, G. Cooperman, M. Cortés-Giraldo, G. Cosmo, G. Cuttone, G. Depaola, L. Desorgher, X. Dong, A. Dotti, V. Elvira, G. Folger, Z. Francis, A. Galoyan, L. Garnier, M. Gayer, K. Genser, V. Grichine, S. Guatelli, P. Guèye, P. Gumplinger, A. Howard, I. Hřivnáčová, S. Hwang, S. Incerti, A. Ivanchenko, V. Ivanchenko, F. Jones, S. Jun, P. Kaitaniemi, N. Karakatsanis, M. Karamitros, M. Kelsey, A. Kimura, T. Koi, H. Kurashige, A. Lechner, S. Lee, F. Longo, M. Maire, D. Mancusi, A. Mantero, E. Mendoza, B. Morgan, K. Murakami, T. Nikitina, L. Pandola, P. Paprocki, J. Perl, I. Petrović, M. Pia, W. Pokorski, J. Quesada, M. Raine, M. Reis, A. Ribon, A. Ristić Fira, F. Romano, G. Russo, G. Santin, T. Sasaki, D. Sawkey, J. Shin, I. Strakovsky, A. Taborda, S. Tanaka, B. Tomé, T. Toshito, H. Tran, P. Truscott, L. Urban, V. Uzhinsky, J. Verbeke, M. Verderi, B. Wendt, H. Wenzel, D. Wright, D. Wright, T. Yamashita, J. Yarba, H. Yoshida, Recent developments in geant4, Nuclear Instruments and Methods in Physics Research Section A: Accelerators, Spectrometers, Detectors and Associated Equipment 835 (2016) 186–225.

doi:https://doi.org/10.1016/j.nima.2016.06.125.
URL https://www.sciencedirect.com/science/article/pii/S0168900216306957

[6] T. Sato, Y. Iwamoto, S. Hashimoto, T. Ogawa, T. Furuta, S. ichiro Abe, T. Kai, P.-E. Tsai, N. Matsuda, H. Iwase, N. Shigyo, L. Sihver, K. Niita, Features of particle and heavy ion transport code system (phits) version 3.02, Journal of Nuclear Science and Technology 55 (6) (2018) 684–690. doi:10.1080/00223131.2017.1419890.

[7] Y. Iwamoto, T. Sato, S. Hashimoto, T. Ogawa, T. Furuta, S. ichiro Abe, T. Kai, N. Matsuda, R. Hosoyamada, K. Niita, Benchmark study of the recent version of the phits code, Journal of Nuclear Science and Technology 54 (5) (2017) 617–635. doi:10.1080/00223131.2017.1297742.

[8] G. Battistoni, J. Bauer, T. T. Boehlen, F. Cerutti, M. P. W. Chin, R. Dos Santos Augusto, A. Ferrari, P. G. Ortega, W. Kozłowska, G. Magro, A. Mairani, K. Parodi, P. R. Sala, P. Schoofs, T. Tessonnier, V. Vlachoudis, The fluka code: An accurate simulation tool for particle therapy, Frontiers in oncology 6 (2016) 116. doi:10.3389/fonc.2016.00116.

[9] e. a. C.J. Werner, Mcnp6.2 release notes, Los Alamos National Laboratory, report LA-UR-18-20808 (2018).

[10] D. Satoh, D. Moriguchi, T. Kajimoto, H. Uehara, N. Shigyo, M. Ueyama, M. Yoshioka, Y. Uozumi, T. Sanami, Y. Koba, M. Takada, N. Matsufuji, Measurement of neutron-production double-differential cross-sections on carbon bombarded with 290-mev/nucleon carbon and oxygen ions, Nuclear Instruments and Methods in Physics Research Section A: Accelerators, Spectrometers, Detectors and Associated Equipment 644 (1) (2011) 59–67. doi:10.1016/j.nima.2011.04.054.
URL https://www.sciencedirect.com/science/article/pii/S0168900211008382

[11] K. Shin, K. Hibi, M. Fujii, Y. Uwamino, T. Nakamura, Neutron and photon production from thick targets bombarded by 30-mev p, 33-mev d, 65-mev ^{3}He, and 65-mev α ions: Experiment and comparison with cascade monte carlo calculations, Phys. Rev. C 29 (1984) 1307–1316. doi:10.1103/PhysRevC.29.1307.

[12] D. Dhar, S. N. Roy, T. Bandyopadhyay, P. K. Sarkar, Measurement and analysis of neutron spectra from thick targets of al and ti bombarded by 30–50 mev α particles, Phys. Rev. C 67 (2003) 024607. doi:10.1103/PhysRevC.67.024607.

[13] K. Sugihara, N. Shigyo, E. Lee, T. Sanami, K. Tanaka, Measurement of thick target neutron yields from 7 mev/u α incidence on 209bi, Nuclear Instruments and Methods in Physics Research Section B: Beam Interactions with Materials and Atoms 470 (2020) 15–20. doi:10.1016/j.nimb.2020.02.037.
URL https://www.sciencedirect.com/science/article/pii/S0168583X20300963

[14] P.-E. Tsai, L. H. Heilbronn, B.-L. Lai, Y. Iwata, T. Murakami, R.-J. Sheu, Thick target neutron yields from 100- and 230-mev/nucleon helium ions bombarding water, pmma, and iron, Nuclear Instruments and Methods in Physics Research Section B: Beam Interactions with Materials and Atoms 449 (2019) 62–70. doi:10.1016/j.nimb.2019.04.030.
URL https://www.sciencedirect.com/science/article/pii/S0168583X19302149

[15] Z. Sun, W.-L. Zhan, Z.-Y. Guo, G. Xiao, J.-X. Li, Ribll, the radioactive ion beam line in lanzhou, Nuclear Instruments and Methods in Physics Research Section A: Accelerators, Spectrometers, Detectors and Associated Equipment 503 (3) (2003) 496–503. doi:10.1016/S0168-9002(03)01005-2.
URL https://www.sciencedirect.com/science/article/pii/S0168900203010052

[16] J. F. Ziegler, M. Ziegler, J. Biersack, Srim – the stopping and range of ions in matter (2010), Nuclear Instruments and Methods in Physics Research Section B: Beam Interactions with Materials and Atoms 268 (11) (2010) 1818–1823, 19th International Conference on Ion Beam Analysis. doi:10.1016/j.nimb.2010.02.091.
URL https://www.sciencedirect.com/science/article/pii/S0168583X10001862

[17] R. Brun, F. Rademakers, Root — an object oriented data analysis framework, Nuclear Instruments and Methods in Physics Research Section A: Accelerators, Spectrometers, Detectors and Associated Equipment 389 (1) (1997) 81–86, new Computing Techniques in Physics Research V. doi:10.1016/S0168-9002(97)00048-X.
URL https://www.sciencedirect.com/science/article/pii/S016890029700048X

[18] D. Satoh, S. Kunieda, Y. Iwamoto, N. Shigyo, K. Ishibashi, Development of scinful-qmd code to calculate the neutron detection efficiencies for liquid organic scintillator up to 3 gev, Journal of Nuclear Science and Technology 39 (sup2) (2002) 657–660. doi:10.1080/00223131.2002.10875185.

[19] T. Kajimoto, N. Shigyo, T. Sanami, K. Ishibashi, R. C. Haight, N. Fotiades, Measurement of absolute response functions and detection efficiencies of an ne213 scintillator up to 600mev, Nuclear Instruments and Methods in Physics Research Section A: Accelerators, Spectrometers, Detectors and Associated Equipment 665 (2011) 80–89. doi:10.1016/j.nima.2011.11.055.
URL https://www.sciencedirect.com/science/article/pii/S0168900211020997

[20] T. Kurosawa, N. Nakao, T. Nakamura, H. Iwase, H. Sato, Y. Uwamino, A. Fukumura, Neutron yields from thick c, al, cu, and pb targets bombarded by 400 mev/nucleon ar, fe, xe and 800 mev/nucleon si ions, Phys. Rev. C 62 (2000) 044615. doi:10.1103/PhysRevC.62.044615.

[21] D. SATOH, T. SATO, A. ENDO, Y. YAMAGUCHI, M. TAKADA, K. ISHIBASHI, Measurement of response functions of a liquid organic scintillator for neutrons up to 800 me v, Journal of Nuclear Science and Technology 43 (7) (2006) 714–719. doi:10.1080/18811248.2006.9711153.

[22] D. Satoh, T. Kurosawa, T. Sato, A. Endo, M. Takada, H. Iwase, T. Nakamura, K. Niita, Reevaluation of secondary neutron spectra from thick targets upon heavy-ion bombardment, Nuclear Instruments and Methods in Physics Research Section A: Accelerators, Spectrometers, Detectors and Associated Equipment 583 (2) (2007) 507–515. doi:10.1016/j.nima.2007.09.023.
URL https://www.sciencedirect.com/science/article/pii/S0168900207020049

[23] J. K. Dickens, Scinful: A monte carlo based computer program to determine a scintillator full energy response to neutron detection for e/sub n/ between 0. 1 and 80 mev: Program development and comparisons of program predictions with experimental datadoi:10.2172/7166672.
URL https://www.osti.gov/biblio/7166672

[24] D. Mancusi, A. Boudard, J. Cugnon, J.-C. David, P. Kaitaniemi, S. Leray, Extension of the liège intranuclear-cascade model to reactions induced by light nuclei, Phys. Rev. C 90 (2014) 054602. doi:10.1103/PhysRevC.90.054602.
URL https://link.aps.org/doi/10.1103/PhysRevC.90.054602

[25] D. Mancusi, K. Niita, T. Maruyama, L. Sihver, R. O. for Information Science, T.-m. Technology, F. College of Bioresource, Nihon Unniversity, C. U. o. T. G. S. Nuclear Engineering, Applied Physics, C. S. Department of Mathematics, S. V. Physics, Roanoke College, Stability of nuclei in peripheral collisions in the jaeri quantum molecular dynamics model, Physical Review. C, Nuclear Physics 79 (1). doi:10.1103/PHYSREVC.79.014614.
URL https://www.osti.gov/biblio/21199512